Draft version January 30, 2017
Preprint typeset using LaTeX style emulateapj v. 01/23/15

arXiv:1701.07932v1 [astro-ph.CO] 27 Jan 2017

SEARCHING FOR THE 3.5 KEV LINE IN THE DEEP FIELDS WITH CHANDRA: THE 10 MS OBSERVATIONS

Nico Cappelluti[1,2,3], Esra Bulbul[4], Adam Foster[5], Priyamvada Natarajan[1,2,3], Megan C. Urry[1,2,3], Mark W. Bautz[4], Francesca Civano[5], Eric Miller[4], and Randall K. Smith[5]

Draft version January 30, 2017

ABSTRACT

In this paper we report a 3σ detection of an emission line at $\sim$3.5 keV in the spectrum of the Cosmic X-ray Background using a total of $\sim$10 Ms Chandra observations towards the COSMOS Legacy and CDFS survey fields. The line is detected with an intensity is $8.8 \pm 2.9 \times 10^{-7}$ ph cm^{-2}s^{-1}. Based on our knowledge of *Chandra*, and the reported detection of the line by other instruments, we can rule out an instrumental origin for the line. We cannot though rule out a background fluctuation, in that case, with the current data, we place a 3σ upper limit at 10^{-6} ph cm^{-2}s^{-1}. We discuss the interpretation of this observed line in terms of the iron line background, S XVI charge exchange, as well as arising from sterile neutrino decay. We note that our detection is consistent with previous measurements of this line toward the Galactic center, and can be modeled as the result of sterile neutrino decay from the Milky Way when the dark matter distribution is modeled with an NFW profile. In this event, we estimate a mass m$_s$ $\sim$7.02 keV and a mixing angle $\sin^2(2\theta) = 0.69$–2.29×10^{-10}. These derived values of the neutrino mass are in agreement with independent measurements toward galaxy clusters, the Galactic center, and M31.

1. INTRODUCTION

Astrophysical and cosmological observations of gravitational interactions of visible baryonic matter provide overwhelming evidence for the existence of an additional dominant, component of non-luminous matter, referred to as dark matter. Extensive direct searches for this ubiquitous matter have so far failed to detect it, and, its nature remains unknown. The majority of this unseen component is inferred to be cold and collisionless, however, a warmer component can also be accommodated to account at least partially to the overall mass budget of dark matter. X-ray observations of dark matter-dominated objects, such as galaxies and clusters of galaxies, provide a unique laboratory for searching for the decay or annihilation of a viable warm dark matter candidate, namely sterile neutrinos (Dodelson & Widrow 1994; Abazajian et al. 2001; Boyarsky et al. 2006).

The recent detection of an unidentified emission line near 3.5 keV in the stacked observations of galaxy clusters, in the nearby Andromeda galaxy (Bulbul et al. 2014a; Boyarsky et al. 2014, Bul14a and Bo14 hereafter). The interpretation of that signal as a decaying dark matter, have drawn considerable attention from astrophysics and particle physics communities. The line is also detected in the *Suzaku* observations of the core of the Perseus cluster (Urban et al. 2015; Franse et al. 2016) and in the Galactic center (Boyarsky et al. 2015). An emission line at a consistent energy is also detected in *XMM-Newton* observations of the Galactic center and in other individual clusters (Iakubovskyi et al. 2015). Recently, a 11σ-detection of the line was reported in summed *NuSTAR* observations of the COSMOS and Extended Chandra Deep Field South (ECDFS) survey fields, where a dark matter signal from the Milky-Way halo may be expected (Neronov et al. 2016). As noted, another interesting other dark matter candidate that might also produce a 3.5 keV X-ray line is self interacting dark matter from relatively low mass axion (e.g., Finkbeiner & Weiner 2007, 2014; Conlon & Day 2014).

Although the line was detected by several X-ray satellites, including *XMM-Newton, Chandra, Suzaku*, and *NuSTAR* in a variety of dark matter-dominated objects, several other studies have also reported non-detections of the line, e.g. in stacked *Suzaku* observations of clusters of galaxies (Bulbul et al. 2016b), the dwarf galaxy Draco (Ruchayskiy et al. 2016), and *Hitomi* observations of the Perseus cluster (Hitomi Collaboration et al. 2016). The upper limits that these non-detections provide are consistent with the detection in stacked clusters of galaxies reported by Bul14 provided the appropriate mass scaling in decaying dark matter models is taken into account (see Abazajian 2016). However, the upper limits derived from the stacked galaxies are in tension with the original detection at the 5σ level (Anderson et al. 2015).

Despite these intensive and persistent efforts, the origin of the 3.5 keV line remains unclear. Potential astrophysical interpretations were discussed extensively by Bul14. The most recent update is provided by Franse et al. (2016), who consider among other models to the charge exchange between bare Sulfur ions and neutral gas (see also Gu et al. 2015; Shah et al. 2016). The radial distribution of the flux of the line can provide an independent test of its origin; however, the observed line flux from the Perseus core is consistent with a dark

[1] Yale Center for Astronomy and Astrophysics, P.O. Box 208121, New Haven, CT 06520, USA.

[2] Department of Physics, Yale University, P.O. Box 208121, New Haven, CT 06520, USA.

[3] Department of Astronomy, Yale University, PO Box 208101, New Haven, CT 06520, USA.

[4] Kavli Institute for Astrophysics & Space Research, Massachusetts Institute of Technology, 77 Massachusetts Ave, Cambridge, MA 02139, USA.

[5] Harvard-Smithsonian Center for Astrophysics, 60 Garden Street, Cambridge, MA 02138, USA

matter origin as well as with an unknown astrophysical line. Furthermore, the intensity of the signal in the cluster core appears to be anomalously high for the decaying dark matter model (Bul14a, Franse et al. 2016). In their recent paper, the *Hitomi* collaboration reports tension between the flux in the Perseus cluster observed by *XMM-Newton* and *Hitomi* at the 3σ level. The authors attribute this discrepancy to subtle instrumental features which may remain in the lower spectral resolution *XMM-Newton* observations of the Perseus cluster even after careful modeling.

Here, we report the detection of the a line at ∼3.5 keV in the summed data from deep *Chandra* blank fields, the *Chandra* Deep Field South (CDFS) and COSMOS for a total exposure of 9.17 Ms. We critically discuss instrumental effects together with four plausible explanations for the origin of the 3.5 keV line, namely, charge exchange, the iron line background, a statistical fluctuation and dark matter decay. All errors quoted throughout the paper correspond to 68% single-parameter confidence intervals; upper limits are at 68% confidence, unless otherwise stated. Throughout our analysis we used a standard ΛCDM cosmology adopting the following values for the relevant parameters: H_0 =71 km s^{-1} Mpc^{-1}, $\Omega_M = 0.27$, and $\Omega_\Lambda = 0.73$.

2. DATA SETS

The *Chandra*-COSMOS Legacy Survey (hereafter, CCLS; Scoville et al. 2007; Elvis et al. 2009; Civano et al. 2016) and the *Chandra*-Deep Field South (hereafter CDFS; Giacconi et al. 2002; Luo et al. 2008; Xue et al. 2011; Luo et al. 2016) have been observed for ∼4.6 M and ∼7 Ms respectively, with the ACIS-I CCD instrument onboard *Chandra* with 117, 111 and 20 pointings, respectively. The CCLS field is a relatively shallow mosaic of ∼2 deg^2 and an average exposure of ∼160 ks/pix while, the CDFS field is a deep pencil beam survey of ∼0.1 deg^2 observed for 7 Ms/pix. However, since the signal is very faint, for spectral analysis we have only used the pointings observed in the VFAINT telemetry mode with a focal plane temperature of 153.5 K, in order to minimize the instrumental background. Since the CDFS was partly observed in the early phase of the mission when the VFAINT mode wasn't available and observations were partly taken at higher temperature, the total exposure time before treatment is ∼6 Ms. We have initially employed also the HDFN 2Ms data, however, after excluding FAINT mode, high temperature data and *cleaned* the data (see below) we ended with only ∼700 ks of usable data that were too noisy for our purposes.

3. DATA ANALYSIS

Raw event files were calibrated using the CIAO tool *chandra_repro* and the Calibration Data Base (CALDB) version 4.8. For every pointing, time intervals with high background were cleaned using the CIAO tool *deflare* using the *lc_clean* technique as described by Hickox & Markevitch (2006). The de-flaring was performed in the [2.3-7] keV, [9.5-12] keV and [0.3-3] keV energy band in sequence, in order to detect flares with anomalous hardness ratios (Hickox & Markevitch 2006). Although not critical for this work, the astrometry was aligned using reference optical catalogs.

The X-ray signal is a blend of detected and unresolved AGN, galaxies and clusters whose summed emission is often referred to as the "Cosmic X-ray Background" (CXB). There is also a particle-induced background and a (relatively small) background from other sources within the instrument. Hereafter we will use the acronym CXB for the signal produced by all astrophysical sources that is focused by the optics and we adopt the acronym PIB for the "Particle and Instrumental Background " which is produced by all other (non-astrophysical) sources.

For sake of clarity, in this paper, the putative 3.5 keV signal arising either from dark matter decay or Sulfur charge exchange, will be considered as a separate component on top of the CXB and PIB signal. Therefore, we start the analysis by carefully accounting for known X-ray sources, that constitute the PIB and the CXB.

3.1. *Extraction of Summed X-ray Spectrum*

The intensity of the CXB is not the same across the surveys presented here, primarily due to cosmic variance, so we derive a separate spectrum for each survey field. For each pointing, we extracted the spectrum of all the photons detected in the ACIS-I field of view (FOV) with the CIAO tool *specextract*. For each spectrum, we then computed the field-averaged Redistribution Matrix Functions (RMFs) and Ancillary Response Functions (ARF) using the CIAO-tool *specextract*. Spectra were co-added and response matrices averaged after weighting by the exposure time. We produced a cumulative CXB+PIB spectrum for each of the datasets. Because we are looking for diffuse emission, the only background component in our observations is the PIB. The *Chandra* X-ray observatory periodically obtains "dark frames", i.e. exposures with ACIS in the stowed mode. When the High Resolution Camera is on the focal plane, ACIS is stowed and unexposed to any focused source but it still records the PIB component. In such a position the ACIS detectors see neither the sky nor the calibration sources. In particular, Hickox & Markevitch (2006) demonstrated that the [2-7] keV to [9.5-12] keV hardness ratio is constant (within 2%) in time regardless of the amplitude of the particle background. Therefore, we employed ACIS-I observations in the stowed mode to evaluate the background. In particular, we merged the *stowed* mode event files, applied the VFAINT filtering, reprojected to the same astrometric frame as the observations, extracted the spectrum in the same source-masked regions and renormalized it by the ratio $C_{[9.5-12],obs}/C_{[9.5-12],stow}$ where $C_{[9.5-12],obs}$ and $C_{[9.5-12],stow}$ are the count rates in the [9.5-12] keV window in the observation and in the *stow* mode data. In a recent paper, Bartalucci et al. (2014) performed a detailed and sophisticated analysis of the same stowed ACIS-I event files employed here and reported, to within 2%, the relative stability of the background in observations of later epochs than those used by (Hickox & Markevitch 2006). In this paper, we are looking for astrophysical emission lines in the energy range [2.4-7] keV, and in this energy band, the PIB is affected by a systematic uncertainty of the order of 2% which is added in quadrature to the PIB spectral data error bars throughout our analysis. In Table 1, we summarize the number of net counts used for the spectral modeling and the resulting vignetting-weighted final exposures for our

TABLE 1
[2.4-7] KEV NET COUNTS AND EXPOSURES

	SIGNAL	BACKGROUND	EXPOSURE
			Ms
CDFS	115373	1989189	5.57
CCLS	131826	1220611	3.59
Total	247199	3209800	9.16

datasets. However, we note that the observations in the stowed mode are much shorter than the those employed here (a total of 1 Ms in the archive vs 9.16 Ms). This of course, significantly limits our sensitivity, since the PIB spectrum has larger errors than those in the data and therefore might potentially artificially smooth out any features in the data.

3.2. *Analysis of the PIB*

Part of the signal included in the total X-ray spectrum is due to the PIB. In order to find faint sources and/or to analyze faint, diffuse, emission-line signals, careful treatment of these backgrounds is essential. We start by examining data from ACIS-I in stowed mode, i.e., when no cosmic photons are collected. This provides a robust representation of the particle background plus internal instrumental background. We model this PIB using a broken power-law, with the slopes (γ_1, γ_2); the break energy (E_{break}) and the normalization (*norm*) as free parameters. On top of this, we add a Gaussian model at $E_1 \sim 2.5$ keV and $E_1 \sim 5.9$ keV, with energies and intensities ($I_{1,2}$) that are free to vary. The line at 5.9 keV is a known Mn K_α instrumental feature. This feature is scattered light from the radioactive ^{55}Fe source in external calibration source. This source has a half-life of ∼2.7years, so its intensity has dropped dramatically over the course of the Chandra mission. So its not surprising that it (and the K-esc and Ti line) isnt fully subtracted from the CXB spectrum. The line at 2.51 keV is instrumental and an artifact: Bartalucci et al. (2014) pointed out that in the [2-3] keV energy band, due the position dependent charge transfer inefficiency (CTI) correction the strong broad emission line at ∼2.1 keV (*mother line*) produces a system of spurious *daughter lines* at energies of up to ∼2.6 keV along with spurious broadening. A similar effect is observed above 7.3 keV as well. CTI correction is necessary because radiation has damaged the ACIS-I resulting in loss in the charge transfer inefficiency. This damage however did not affect areas of the CCD not exposed to the X-rays such as the frame store area. To cope with the CTI, a correction is applied *a posteriori* by the data analysis pipeline. This correction is applied to all the data including those collected by areas not damaged by radiation. The result is that for the strongest instrumental emission lines, the recorded energy is artificially shifted up to 800 eV higher energy (depending on the position on the detector).

XSPEC v12.9.0 was used to perform the spectral fits with the extended C-statistic as an estimator of the goodness-of-fit. We restricted the energy range to 2.4–7 keV in order to avoid the bright *Au* feature at 2 keV, while having sufficient leverage on the power-law component. We show in Table 2 the best-fit parameters and 90% uncertainties on the derived background parameters for the CCLS field which are used as a reference for the other fits. Together with the best-fit parameters obtained, we show that in the model normalization for the two fields, there is an indication of the mean particle radiation level during the observations. The model gives a good-fit with a corresponding total χ^2 of 102.75 for 123 dof. Figure 1 shows the modeled stowed ACIS-I PIB spectrum. For the CDFS the shape of the PIB is basically identical except for the overall amplitude. However, we point out that when modeling the spectrum there is lot of uncertainty on the shape of the continuum which may raise concern. In particular, our best fit shows a break in the PIB spectrum at ∼3.77 which is less than two resolution elements away from the line that we are searching for. Moreover, the fit of the soft power-law component of the continuum has been derived in a region of the spectrum where Bartalucci et al. (2014) noticed several additional CTI features (see above). Accounting for these, after a careful evaluation of the PIB we consider it safer and more conservative to directly subtract the observed PIB from the data rather that modeling it (but see Section 4.1). We also modeled the PIB continuum by using the model proposed by Bartalucci et al. (2014) (i.e. an exponential decay plus a power law) but the continuum turns out to be slightly overestimated in [3-4] keV band.

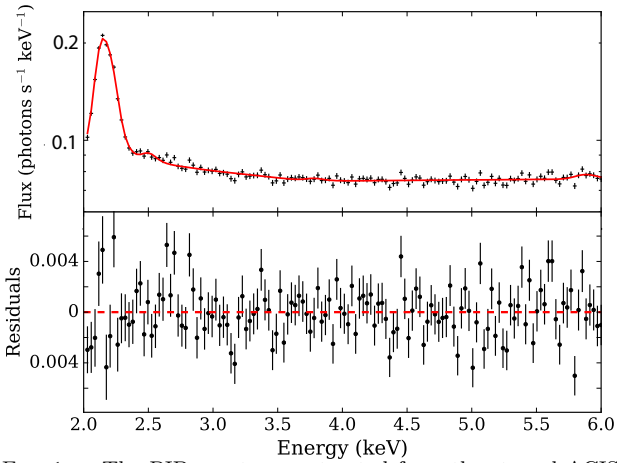

FIG. 1.— The PIB spectrum extracted from the stowed ACIS-I observations and matched to CCLS data is shown. The best-fit model is marked in red.

4. RESULTS

To increase the sensitivity to weak emission lines, we simultaneously fit the CXB spectra from the CCLS and CDFS in the [2.4-7] keV energy band. The Galactic column densities are fixed to 2.5×10^{20} cm^{-2} for the fits of the CCLS field and 8.8×10^{19} cm^{-2} for the CDFS field (Dickey & Lockman 1990). We first fit the spectra in the [2.4-7] keV band with a single absorbed (*wabs* model in XSPEC) power-law model which gives an overall good fit with χ^2 of 542.43 for 290 degrees-of-freedom (dof). The power-law indices are fixed to 1.4, while the normalizations are left free in our fits to account for the different CXB flux in the two fields (Hickox & Markevitch 2006). The best-fit power-law normalizations are found to be: ∼1.53 $\times10^{-4}$ ph keV^{-1} cm^{-2} s^{-1} in CDFS

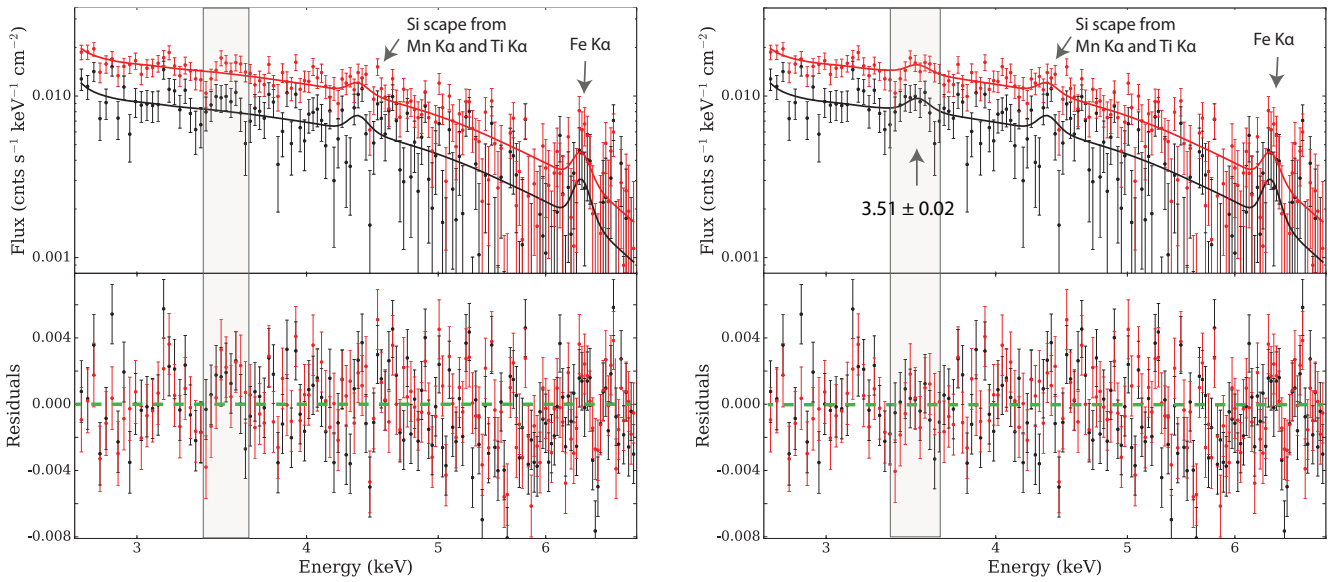

FIG. 2.— **Left Panel** : The CXB spectra in the CDFS (*in black*) and CCLS (*in red*) together with best-fit models (solid lines) and the residuals without the 3.5 keV line Gaussian model component. **Right Panel** : the same by adding a Gaussian model at ∼3.5 keV. The known instrumental lines Si escape peak from Mn Kα, Ti Kα at 4.4 keV and Fe Kα at 6.4 keV are marked in both panels..

and 2.03×10^{-4} ph keV^{-1} cm^{-2} s^{-1} in CCLS. At first instance, our measurements of the CDFS is in agreement with Hickox & Markevitch (2006), Moretti et al. (2012) and Bartalucci et al. (2014) while, for CCLS an extensive discussion of the CXB intensity is presented by Cappelluti et al. (2017).

We show the best fit and residuals in Figure 2. A few spectral features are immediately visible at 2.51 keV, 3.5 keV, 4.4 keV and 6.4 keV. We now discuss each of these detected features. In the top panel we present the best fit obtained without the 3.5 keV line in the model while the lower panel shows the effect of including the line. The line at 6.4 keV is consistent with the Fe K_α that can either have an instrumental or a Galactic origin. The 4.37 keV lines are consistent with a residual from a blend of known instrumental emission lines from Silicon escape (i.e. lines formed by electron clouds left when a photon carrying away energy E leaves silicon substrate)[6] from Mn $K_{\alpha_{1,2}}$ and Ti $K_{\alpha_{1,2}}$ [7] given that the energy resolution is >200 eV at these energies. These line can be produced from the on-board external calibration source. These two weak emission lines are hard to detect in the PIB but they become clearly visible with the deep integrations used here and their residuals become evident. Adding these Gaussian components with variable energy and normalization for each field to the total fit improves the total χ^2 value by a significant amount with $\Delta\chi^2$ of 509.76. for 7 extra dof. The best-fit energy of the Gaussian around the 3.5 keV line becomes $3.51^{+0.02}_{-0.02}$ keV with a flux of $8.83\pm2.9\times10^{-7}$ ph cm^2 s^{-1}. If this line is removed from the fit the change in χ^2 value becomes 9.22 ($\Delta\chi^2$ of 9.22) for 2 dof, corresponding to a detection confidence level of 3σ. We point out that fits performed with CSTAT produce very similar results.

[6] http://cxc.harvard.edu/cal/Acis/Cal_prods/matrix/notes/Flesc.html

[7] http://www2.astro.psu.edu/xray/docs/cal_report/node155.html

4.1. *Safety tests*

For comparison, we repeated the same fit with the same model but instead of directly subtracting the background in XSPEC (as is usually done in the literature and done above), we now include a background model with the best-fit model parameters obtained from the fits to the PIB in each field (see Section 3.2). The energies of the Gaussian components and the break energy of the power-law component are fixed to the values obtained from the PIB data, while the normalizations are left free. The fit produced a result consistent with the case where the background is directly subtracted.

As further test we fitted the spectrum obtained after masking all the known sources in the field. At the time of the analysis the latest public catalog of CDFS sources was produced with the 4 Ms exposure of Xue et al. (2011) so we have mosaicked all the available observations, produced exposure maps as described by Cappelluti et al. (2016), and run a source detection with *wavdetect* in the [0.5-2] keV, [2-7] keV and [0.5-7] keV energy bands. We set a threshold at 10^{-5} and the faintest detected sources have fluxes of the order 10^{-17} erg cm^{-2} s^{-1}. For each source, we created regions with a spatial extent of 5σ of the PSF around the centroid (ranging from $\sim1''$ FWHM at the center of the image to $>5''$ at the outskirts). The three-band catalogs were merged and sources in each of the bands were removed from the event files of each pointing[8]. CCLS has a completely different tiling of pointings and the source detection requires a more complicated approach. For this reason we employed the catalog published by Civano et al. (2016) and, for each CCLS pointing we mask sources within $\sim10''$ around each detection. According to Fig. 9 of Civano et al. (2016), this procedure will safely remove >90% of the sources' flux in the energy bands investigated here. We repeated the pro-

[8] A few days before the submission of the paper, Luo et al. (2016) presented the CDFS 7 Ms catalog, there is a substantial agreement between our mask and their catalog.

cedure described above and we still measure a line at $3.51^{+0.03}_{-0.03}$ keV and an intensity of $8.27\pm4.3 \times 10^{-7}$ ph cm^2 s^{-1}, consistent with the detection using the whole data set but significant at just about 2σ. This is due to the fact that the source masking, especially in the CDFS, removes a larger fraction of the data (>50%) and hence the statistics on the continuum is severely affected.

Considering the marginal significance of the detection we asked ourselves if the detected 3.5 keV line was a statistical fluctuation? As far as the 3.5 keV line is concerned, this is not a blind search since the energy of line under investigation is known a-priori. This means that the *look elsewhere effect* in our measurement is not important or at least negligible. However, given the low Signal-To-Noise ratio of the detected signal, we tested the hypothesis that the observed line might be a statistical fluctuation in the background. In order to test this, we obtained 1000 random realizations of the best fit spectrum without the 3.5 keV line via Monte-Carlo integration. At the same time we also drew 1000 random realizations of the stowed background spectrum. With these datasets in hand we fitted every realization with the model including the 3.5 keV line. We searched how many times the χ^2 improved by at least $\Delta\chi^2$=9.22 which corresponds to our detection. With this cut, the line was falsely detected only once - which corresponds to a 0.1% probability of false detection. However since the background level is known with a ∼2% precision, we cannot at the moment exclude that systematic effects could indeed produce the observed line, however we point out that in the [3–4] keV band the overall spectrum is rather flat and the effective area is rather smooth. In any case, according to our simulation, if our detection turns out to be a fluke, at the 3σ upper-limit we can determine that the 3.5 keV line flux is $<10^{-6}$ ph cm^2 s^{-1}. Additional we compute the 3σ, 3.51 keV line, upper limit in the HDFN data. This was $<2.7\times10^{-6}$ ph cm^2 s^{-1}

5. DISCUSSION

We discuss our findings in the context of earlier claims of detection of the 3.5 keV line by several other groups. The 3.5 keV line has been previously detected in the in the direction of the Perseus Cluster; in a stack of galaxy clusters, and more recently, toward the Galactic Center and in M31 by Bo14. Interestingly, the energy of the line is consistent with that detected in Perseus redshifted from z=0.018. However, the recent non-detection by *Hitomi* (Hitomi Collaboration et al. 2016) rules out the highest flux detected by XMM-MOS in the the direction of Perseus. Recently, Perez et al. (2016) questioned the detection of the 3.5 keV line in the Galactic center with NuSTAR, however their *internal* background model contained a line at 3.54 keV, introduced in Table 5 of Wik et al. (2014) but was never explained because of the relatively poor calibration of NuSTAR around 3-4 keV. We note that it is possible that the line would have been detected if it had not been modelled as a background feature.

In a recent paper, Neronov et al. (2016) reported a 11 σ detection of the 3.5 keV line in NuSTAR observations of the CCLS field and the CDFS. They observed the same areas of sky observed here, for a comparable exposure time, taking advantage of the fact that the NuSTAR detector which was not shielded from indirect light, was able to effectively survey a total sky area of 37.2 deg^2 viewed by a $13'\times13'$ detector area. This obviously provides increased leverage compared to telescopes sensitive to focused photons only. Interestingly, the line has been detected by Wik et al. (2014) but no hypothesis has been put forward for its origin. In fact, the line has been flagged as instrumental. Chandra and NuSTAR have the same collecting area at 3.5 keV and the exposures used in these two papers are comparable. We can therefore, directly compare the two results by transforming the observed fluxes into surface brightness (S) under the assumption that the line flux is homogenous over the 37.5 deg^2, however for NuSTAR ($S_{3.5,Nu}$) we have to take into effect the boosting factor introduced by the non-focused component of the signal so that:

$$S_{3.5,Nu} = F_{3.5,Nu}/(\kappa(E) * 1.43 \times 10^{-5}), \qquad (1)$$

where $F_{3.5,Nu}$ is the flux of the line observed by NuSTAR and $\kappa(E)$ is the energy dependent $boosting factor$ for the NuSTAR measured diffuse indirect background. This takes into account the fact that the effective surveyed area is much larger than the area sensitive to focused photons.

At 3.5 keV, Neronov et al. (2016) report $\kappa(E)$ ∼7.5 and the field of view (f.o.v.) of the Cd Zn Te detector is 1.43×10^{-5} sr while ACIS-I's f.o.v. is 2.42×10^{-5} sr. Considering this we find $S_{3.5,Nu}$=0.093±0.023 ph/cm^2/s/sr and $S_{3.5,Nu}$=0.069±0.012 ph/cm^2/s/sr with data taken in the shadow of the earth and illuminated by the Sun, respectively and $S_{3.5,Ch}$=0.036±0.012 ph/cm^2/s/sr with Chandra.

Our measurements are thus marginally consistent (at ∼1.9-2σ) with NuSTAR's by Neronov et al. (2016). We cannot exclude that Chandra and NuSTAR are observing the same cosmic source of 3.5 keV photons. However if the flux of the line is as measured by NuSTAR, we would have detected the line at least 5σ. However, it is worth noting that the calibration of the effective area of NuSTAR in that energy band is very unstable (as per information from the NuSTAR Calibration team) and a 2% spike could be introduced by the fact that during the calibration the control points for the Crab fitting are at 3.3 and 3.68 keV, the Crab and hence the response has been corrected between these two energies with a straight line.

If the line is not an artifact, the NuSTAR detection is ∼3 times more significant because they collected 10 times more photons than Chandra did. Assuming a consistency between the measurements (even if marginal), given the differences in satellite orbits and detectors, means an instrumental or cosmic ray origin for the signal is unlikely. The intensity of line is the same both with the spacecraft illuminated by the Sun and in the shade of the Earth. Moreover, *Chandra* observations were taken over ∼ 15 years while NuSTAR data were obtained in just the past 3 years which argues against such transient causes such as the solar wind. However the energy of the line is remarkably consistent with the two observations, taken with two different instrumental setups[9], under different geomagnetic conditions and at completely different times, suggests an extrinsic source for the detected line.

[9] ACIS-I is a silicon CCD while the imagers of NuSTAR are two Cadmium-Zinc-Telluride detectors

TABLE 2
Measured Model Parameters of the PIB Fit

γ_1	γ_2 10^{-2}	E_{break} keV	Norm keV^{-1} cm^{-2} s^{-1}	χ^2 (dof)	E_1 keV	$I_{E_1}{}^2$ ph cm^{-2} s^{-1}	E_2 keV	$I_{E_2}{}^2$ ph cm^{-2} s^{-1}
0.35±0.04	-1.95±2.96	3.77±0.12	(0.12±0.05, 0.18±0.03)[1]	100.62 (123)	$2.51^{+0.06}_{-0.03}$	8.21±2.5	$5.90^{+0.07}_{-0.04}$	$6.49^{+1.78}_{-3.21}$

[a]CCLS and CDFS, respectively.
[b]$\times 10^{-4}$

Hitomi Collaboration et al. (2016) speculated that the line might be a feature of CCD detectors but this would not account for the NuSTAR detection with CdZnTe detectors.

Moreover, a recent analysis of the *Chandra* instrumental background by Bartalucci et al. (2014) did not find any residuals nor emission lines between 3 and 5.8 keV. While we cannot exclude further unaccounted and as yet unknown effects introduced by the mirrors, based on this concordance the instrumental origin seems to be less likely with multiple detections in the data taken with different instruments and under different conditions. A further source of concern is the contamination of ACIS optical blocking filter by a deposit of hydrocarbons. This effect has been known for many years and well understood. Moreover, while this effect is dramatic in the soft bands, it is small above 3 keV and we consider it negligible. We also investigated the possibility that Tin whiskers (crystalline structures of tin growing when tin coatings are used as a finish) might be implicated, since Sn_{50} presents energetic transitions in L shells around 3.5 keV. However, consulting with the Chandra engineering team suggests that the amount of tin is relatively small but we couldn't estimate its contribution to our observations. Still, further calibrations, and deeper studies of the spectral dependence of the instrument response are needed and will be important for firmly establishing the reality (or not) of this emission feature. In particular, we would recommend deeper integrations of the stowed background.

With this analysis we can affirm that unless the Chandra effective area calibration has problems at 3.5 keV that remain undetected despite substantial attention to this energy, we can exclude an instrumental origin for the line. We now proceed to discuss possible physical mechanisms that can produce an emission line at 3.5 keV.

TABLE 3
Best-fit Model Parameters from the Joint Fits of Deep Field CXB Spectra.

Energy keV	Flux 10^{-6} ph cm^{-2} s^{-1}
2.51 ± 0.01	52.80 ± 19.64
3.51 ± 0.02	0.88 ± 0.29
4.37 ± 0.03	1.12 ± 0.29
6.38 ± 0.04	1.98 ± 0.55
C-stat (dof)	514.80 (283)

5.1. *The Iron Line Background*

Regardless of the nature of the search, we know that when observing the CXB, we are witnessing the accretion history onto Super Massive Black Holes across cosmic time. There is evidence that a large fraction of the accretion in the universe occurs in an obscured phase (see e.g., Gilli et al. 2007; Treister & Urry 2005). One characteristic feature of such a phase of accretion is a strong Fe K_α 6.4 keV emission line. Such an emission line has been significantly detected in stacked spectra of AGN divided into redshift bins (see e.g. Brusa et al. 2005; Falocco et al. 2013; Chaudhary et al. 2010), with a very intense contribution from sources at z∼0.7-.0.9 (i.e. Fe K_α redshifted to 3.5 keV) where the cosmic AGN activity was near its peak. However the CXB spectrum contains the emission from AGN from all redshifts and its intensity is modulated by the redshift distribution of the sources and their luminosity distance. Gilli et al. (1998, 1999) modeled this emission and found that the the redshift distribution smooths this signal into an 'inverse edge'-shaped feature between 2 and 4 keV. The intensity of such a feature is a few percent above the continuum at about 3.5 keV, however since the redshift distribution of the resolved sources is not smooth but it shows spikes due to the presence of large scale structure, the feature appears near or at the energy of such spikes. Both COSMOS and the CDFS show spikes in their AGN redshift distribution around z∼0.8 (Luo et al. 2016; Marchesi et al. 2016). Therefore, since the expected intensity of the line is of the order 5-10% above the continuum, we cannot exclude such an origin for the observed 3.5 keV line. On the other hand there is a hint of the line even after removing detected sources: and there is no reason why the unresolved CXB sources should not also spike at the same redshift. Furthermore the fact that the line has been detected at the same energy observed in galaxy clusters and the Galactic center, it is unlikely that the feature is from AGN in the background. Larger collecting area telescopes will help to further investigate such an hypothesis in the future.

5.2. *3.5 keV line from S XVI Charge exchange*

Gu et al. (2015) suggested that the 3.5 keV line could be attributed to Charge Exchange (CX) between neutral Hydrogen and bare Sulfur ions. This collision leads to the full Lyman series of transitions in S XVI, with a strong Ly_α at 2.62 keV and, crucially, enhanced high n transitions around Ly_η and Ly_θ (i.e. $n = 8 \rightarrow 1, 9 \rightarrow 1$) transition. These enhanced high n lines are the indicator of CX, driven by capture into the high n shells which does not occur during electron impact collisional excitation. Significantly for this work, these lines lie in the

3.4–3.45keV energy band.

The exact ratios of the lines in the Lyman series depends on the exact n and l shell into which the electron is captured. In particular, the l shell is very sensitive to the collision energy, although calculations of the relative cross section are sparse and highly likely to disagree. We have used data from the AtomDB Charge Exchange (ACX) model (Smith et al. 2012) to obtain the line energies and relative intensities shown in Table 4. In this case we have used ACX model 8, which is the separable l distribution and the weighted n distribution (described in Smith et al. 2012). This corresponds to relatively low center of mass velocity ($\lesssim$ 1000km/s) which is appropriate for a thermal plasma such as this one, however the results do not change significantly if other distributions are used instead.

In all of these observed scenarios, the intensity of the Lyα line is 5 times that of the 3.4-3.45keV line complex. We do not detect a line with an energy consistent with 2.62 keV, although we can determine an upper limit for its intensity at $< 1 \times 10^{-5}$ ph/cm^2. By assuming that all of the ∼3.5 keV emission is produced by S XVII CX, and considering the energy resolution of Chandra (of the order 150 eV) and NuSTAR (400 eV), we test the hypothesis of Gu et al. (2015) and Shah et al. (2016) that we are seeing a blend of all the possible transitions around 3.4-3.45 keV. Although, the energy of the line detected here is clearly in tension with the predictions for S XVII CX, the discrepancy just might be a consequence of the energy resolution of the instrument.

From the values in Table 4, we expect a line ratio $I_{3.45}/I_{2.62}$ of ≤ 0.2, where $I_{3.45}$ is the intensity of the 3.45 keV line system. In our case the ratio is >0.25, inconsistent with CX and with a discrepant energy. However, any signal at 2.62 keV, that we can interpret here as the n=2→1 S XVII transition can also be attributed to the daughter lines of the instrumental feature at 2.1 keV. Any such contribution would, in effect, raise the observed ratio above 0.2, making CX even less likely. In addition, the CX process should also produce a significant Ly$_\beta$ line at 3.106keV with $I_{3.106}/I_{2.62}$ of ∼0.14. We observe no such line, with a 3σ upper limit of $< 2 \times 10^{-6}$ ph/cm^2/s, $I_{3.106}/I_{2.62}$ >0.2

Another possible CX transition that occurs near 3.5 keV is the Ar XVIII n=2→1 transition at 3.32 keV, where we do not detect any line nor do we see any evidence of higher n shell transitions from this ion. According to these measurements and atomic calculations, we can conclude that, at >3σ confidence level, the totality of the 3.5 keV line flux is not produced by CX.

5.3. *3.5 keV line from dark matter decay*

One of the possible interpretations of the detection of the 3.5 keV emission line is the decay of sterile neutrinos into two photons (Pal & Wolfenstein 1982). If the emission originates from DM decay, then the line flux would be proportional to the amount of matter along the line of sight over the field-of-view.In the present case, we would expect the Milky Way dark matter halo to dominate the local signal. With this data set, we sample the DM halo distribution along the line of sight and therefore, the emission seen should scale with amount of mass sampled.

TABLE 4
PREDICTED S XVI CHARGE EXCHANGE TRANSITIONS LINES.

Transition	Energy keV	$I_{line}/I_{2.62}$
2→1	2.621	1.0
3→1	3.106	0.142
4→1	3.276	0.050
5→1	3.354	0.025
6→1	3.397	0.016
7→1	3.423	0.011
8→1	3.434	0.120
9→1	3.451	0.074

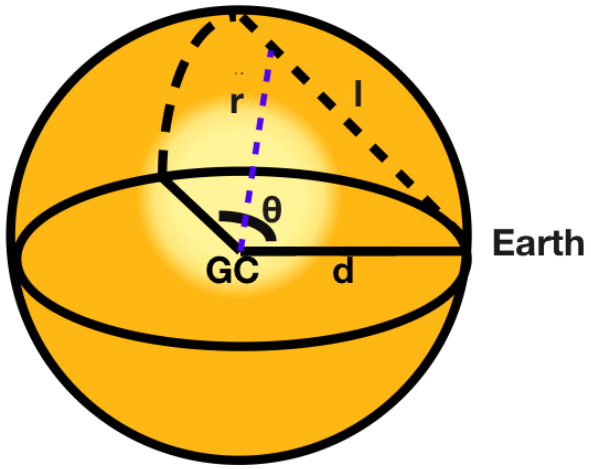

FIG. 3.— A spherical approximation of the problem in Eq. 2, the sphere represents a spherical section of the MW DM halo. The *yellow color* scale represents the DM density which we assume to follow a NFW profile. The circle along the equator of the sphere represents the Galactic plane. d is the distance from Earth to the Galactic Center (GC), l is the distance along the line of sight where we integrate the DM profile at the varying distance r from the GC (blue dashed line). θ is the aperture angle.

Boyarsky et al. (2014), detected the 3.5 keV line in the direction of the GC. The observed fields presented here lie at an aperture angle θ with respect to the GC. If our detected signal comes from DM decay within the MW halo then its intensity should be:

$$S_{DM}(\theta) = S_{DM,GC} \frac{\int \rho_{DM}[r(l, 0^\circ)]}{\int \rho_{DM}[r(l,\theta)]} dl\, d\Omega \qquad (2)$$

where, $S_{DM}(\theta)$ is the DM decay signal at aperture angle θ from the GC; $S_{DM,GC}$ is the DM decay signal from the GC (θ=0); ρ(r) is the DM density profile; l is the distance along the line of sight; r and θ are the physical and angular distance from the center of the galaxy, respectively. The three quantities are related via

$$r(l,\theta) = \sqrt{l^2 + d^2 - 2ldcos(\theta)} \qquad (3)$$

where d is the distance of the earth from the GC. We note that the distance and MW DM profile parameters

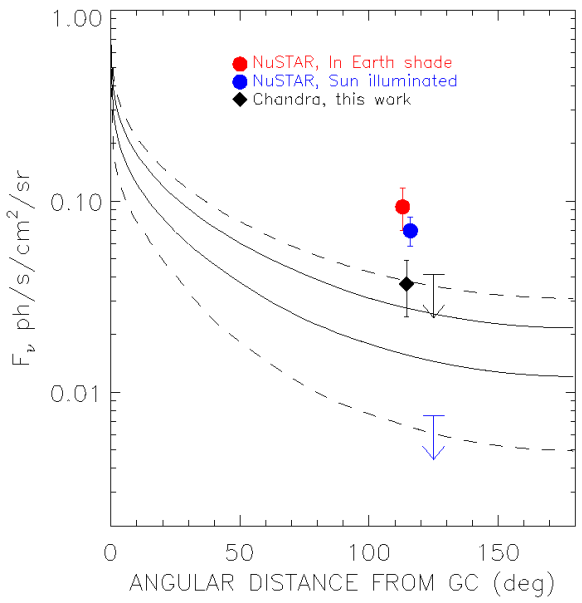

FIG. 4.— 1σ (*continuous line*) and 2σ (*dashed line*) limits on the expected 3.5 keV line flux as function of the angular distance from the GC by assuming a NFW profile with parameters from Nesti & Salucci (2013). The profile is compared with our measurements from the deep fields (*black filled circles*) and with the NuSTAR results (*red/blue filled circles*). The *downward − black* arrow represents the 3σ limit derived from simulations. The *downward − blue* arrow represents the 3σ sensitivity to the 3.5 keV line with 50 Ms Chandra.

and shape are still highly debated (Bland-Hawthorn & Gerhard 2016).

Assuming that all the intervening dark matter is associated with a cold component that can be modeled with an NFW profile (Navarro et al. 1997) given by:

$$\rho_{DM} = \frac{\rho^*}{x(1+x)^2} \tag{4}$$

where $x = r/r_H$; here we adopt the parameters measured by Nesti & Salucci (2013): and therefore use d=8.02±0.2 kpc, r_H=16.1$^{+12.2}_{-5.6}$, ρ^*=13.8$^{+20.7}_{6.6}$ × 10^6 $M_\odot$/kpc^3 and $S_{DM,GC}$=0.63±0.11 ph/s/cm^2/sr. Using Eq. 2 we calculated, with Monte Carlo integration, the 1σ and 2σ confidence levels of the flux from DM decay along the line of sight as a function of the angular distance from the GC. This is shown in Fig. 4, wherein we overplot our measurement and the NuSTAR measurement. The two fields investigated here are basically at the same angular distance from the GC of $\theta \sim$115 deg. Remarkably, our measurements are consistent at the 1σ level with such a profile. This means the ratio of fluxes at θ=115 and θ=0 is consistent with the NFW DM decay model.

In terms of constraints on the number of neutrino species (allowing one additional species of a sterile neutrino along with the 3 other usual flavors), Planck Collaboration et al. (2015) report that with the CMB temperature data alone it is difficult to constrain $N_{\rm eff}$, and data from Planck alone do not rule out $N_{\rm eff} = 4$. At the 95% C.L. combining Planck + WMAP + high l experiments they obtain $N_{\rm eff} = 3.36^{+0.68}_{-0.64}$. The Planck collaboration has only investigated an eV mass sterile neutrino as a potential additional species. So other than saying that $N_{\rm eff} = 4$ is permitted, there are no concrete CMB constraints on keV sterile neutrinos.

Performing the line integral through the halo of the Milky Way taking into account the f.o.v and given that all 3 deep fields included in this analysis are at roughly 115 degrees, we compute the surface mass density along the line of sight. Similar to our assumption adopted above, the MW halo is once again modeled with an NFW profile and the current best-fit parameters are adopted from Nesti & Salucci (2013). Using the formulation developed in Abazajian et al. (2007), we use the measured flux in the line to constrain the mixing angle $\sin^2 2\theta$. Although we use the integrated surface mass density of dark matter in the Milky Way halo integrated out to the virial radius, the dominant contribution comes from the inner region - from within a few scale radii - of the density profile due to the shape of the NFW profile. Using the higher bound and the lower bound estimates for the total mass of the Milky Way, we obtain the following values for Σ the integrated surface mass density of DM:

$$\begin{aligned} \Sigma_{\rm DM,High} &= 0.0362\,{\rm gm\,cm^{-2}}; \\ \Sigma_{\rm DM,Low} &= 0.0109\,{\rm gm\,cm^{-2}}. \end{aligned} \tag{5}$$

Using these values and the equation:

$$\begin{aligned} \sin^2 2\theta \times \left(\frac{m_\nu}{1\,1\,{\rm keV}}\right)^4 \times \frac{\Sigma_{\rm DM}}{\rm gm\,cm^{-2}} = \\ \left(\frac{I_\nu}{1.45\times10^{-4}}\right) {\rm photons\,cm^{-2}\,s^{-1}\,arcsec^{-2}}, \end{aligned} \tag{6}$$

we obtain that $\sin^2 2\theta_{\rm DM,High} = 6.92 \times 10^{-10}$ and $\sin^2 2\theta_{\rm DM,Low} = 2.29 \times 10^{-10}$. Furthermore, we can now estimate the lifetime τ for this sterile neutrino species, using equation 2 of Boyarsky et al. (2015):

$$\tau_{\rm DM} = 7.2 \times 10^{29}\,{\rm sec}\left(\frac{10^{-8}}{\sin^2 2\theta}\right)\left(\frac{1\,{\rm keV}}{m_\nu}\right)^5 \tag{7}$$

and find that it is $\tau_{\rm DM,High} = 6.09 \times 10^{27}$ sec and $\tau_{\rm DM,Low} = 1.83 \times 10^{27}$ sec respectively. These mixing angle estimates are in very good agreement with Figures 13 and 14 of Bul14. They can also be overplotted and seen clearly to be consistent with Figure 3 of Iakubovskyi et al. (2015).

However, despite concordance with parameters extracted from other observational constraints obtained from X-ray data of stacked galaxy clusters and the Galactic center, due to the significance of our detection only at the 3σ level, we cannot conclusively claim that this observed 3.51 keV line originates from decaying dark matter. It would require a non-detection with at least 50 Ms of *Chandra* observations to rule out this hypothesis (see Fig. 4).

6. SUMMARY

In this paper, we have presented a 3σ detection of an unidentified emission feature at ∼3.5 keV in the spectrum of the CXB with extremely deep integration time. Examining the sources of possible origin for this feature, we conclude that the line does not have a clear known instrumental origin. The intensity and the energy of the line is consistent with previous measurements that were

interpreted as decay of ∼7 keV sterile neutrino and the decay rate found here is in remarkable agreement with previous work. We can interpret the signal as DM decay along the line of sight in the Milky Way halo.

We investigate also the scenario where the 3.5 keV flux is produced by with CX between neutral Hydrogen with bare Sulfur ions. we conclude that at $>>3\sigma$ confidence all the 3.5 keV flux cannot be produced by CX. We also discuss a scenario, the line could be produced by a blend of redshifted iron lines from AGN by large scale structures that spike at z∼0.8. This interpretation would be consistent with predictions for the iron line background but not with cluster measurements. So far, the 3.5 keV line is the only feature detected from 4 independent instruments that is interpretable at DM decay (*Chandra*, XMM-*Newton*, *Suzaku* and *NuSTAR*) with more than one >5 σ detection in a variety of DM dominated objects. Given the amount of data available in the archives, an intensive data mining exercise of X-ray spectra is an extremely cost- and time-effective method to rule out or confirm the contribution of sterile neutrinos to DM. The nature of dark matter is a key unsolved problem in cosmology and at the moment we seem to be at an impasse in terms of direct detection experiments (see e.g. Ackermann et al. 2015; IceCube Collaboration et al. 2016). Therefore, further even more careful analysis of existing X-ray observations is warranted and crucial. In the future, X-ray calorimeters on board of *XARM* (X-ray Astronomy Recovery Mission), *Athena* or the Micro-X sounding rocket (Figueroa-Feliciano et al. 2015) will greatly improve our understanding of the origin of the 3.5 keV feature given their capability for high precision spectroscopy.

7. ACKNOWLEDGEMENTS

NC acknowledges the Yale University YCAA Prize fellowship postdoctoral program. PN acknowledges a Theoretical and Computational Astrophysics Network grant with award number 1332858 from the National Science Foundation and thanks the Aspen Center for Physics, which is supported by the National Science Foundation grant PHY-1066293, where this work was done in part. EB acknowledges support from NASA grants NNX13AE77G

REFERENCES

Abazajian, K., Fuller, G. M., & Tucker, W. H. 2001, ApJ, 562, 593
Abazajian, K. N., Markevitch, M., Koushiappas, S. M., & Hickox, R. C. 2007, Phys. Rev. D, 75, 063511
Abazajian, K. N. 2014, Physical Review Letters, 112, 161303
Abazajian, K. N. 20146, to be submitted
Ackermann, M., Ajello, M., Albert, A., et al. 2015, Phys. Rev. D, 91, 122002
Arnaud, K. A. 1996, Astronomical Data Analysis Software and Systems V, 101, 17
Anderson, M. E., Churazov, E., & Bregman, J. N. 2015, MNRAS, 452, 3905
Bartalucci, I., Mazzotta, P., Bourdin, H., & Vikhlinin, A. 2014, A&A, 566, A25
Bland-Hawthorn, J., & Gerhard, O. 2016, ARA&A, 54, 529
Boyarsky, A., Neronov, A., Ruchayskiy, O., Shaposhnikov, M., & Tkachev, I. 2006, Physical Review Letters, 97, 261302
Boyarsky, A., Ruchayskiy, O., Iakubovskyi, D., & Franse, J. 2014, Physical Review Letters, 113, 251301
Boyarsky, A., Franse, J., Iakubovskyi, D., & Ruchayskiy, O. 2015, Physical Review Letters, 115, 161301
Bulbul, E., Markevitch, M., Foster, A., et al. 2014, ApJ, 789, 13
Bulbul, E., Markevitch, M., Foster, A. R., et al. 2014, arXiv:1409.4143
Bulbul, E., Markevitch, M., Foster, A., et al. 2016, ApJ, 831, 55
Brusa, M., Gilli, R., & Comastri, A. 2005, ApJ, 621, L5
Conlon, J. P., & Day, F. V. 2014, J. Cosmology Astropart. Phys., 11, 033
Cappelluti, N., Comastri, A., Fontana, A., et al. 2016, ApJ, 823, 95
Cappelluti, N., et al. 2016, , ApJ, submitted
Carlson, E., Jeltema, T., & Profumo, S. 2015, JCAP, 2, 009
Chaudhary, P., Brusa, M., Hasinger, G., Merloni, A., & Comastri, A. 2010, A&A, 518, A58
Dickey, J. M., & Lockman, F. J. 1990, ARA&A, 28, 215
Dodelson, S., & Widrow, L. M. 1994, Physical Review Letters, 72, 17
Falocco, S., Carrera, F. J., Corral, A., et al. 2013, A&A, 555, A79
Figueroa-Feliciano, E., Anderson, A. J., Castro, D., et al. 2015, ApJ, 814, 82
Finkbeiner, D. P., & Weiner, N. 2014, arXiv:1402.6671
Franse, J., Bulbul, E., Foster, A., et al. 2016, arXiv:1604.01759
Foster, A. R., Ji, L., Smith, R. K., & Brickhouse, N. S. 2012, ApJ, 756, 128
Iakubovskyi, D., Bulbul, E., Foster, A. R., Savchenko, D., & Sadova, V. 2015, arXiv:1508.05186
Jeltema, T., & Profumo, S. 2015, MNRAS, 450, 2143
Finkbeiner, D. P., & Weiner, N. 2007, Phys. Rev. D, 76, 083519
Finkbeiner, D. P., & Weiner, N. 2014, arXiv:1402.6671
Foster, A. R., Ji, L., Smith, R. K., & Brickhouse, N. S. 2012, ApJ, 756, 128
Gilli, R., Comastri, A., Brunetti, G., & Setti, G. 1998, Astronomische Nachrichten, 319, 65
Gilli, R., Comastri, A., Brunetti, G., & Setti, G. 1999, New A, 4, 45
Gilli, R., Comastri, A., & Hasinger, G. 2007, A&A, 463, 79
Gu, L., Kaastra, J., Raassen, A. J. J., et al. 2015, A&A, 584, L11
Hitomi Collaboration et al. 2016, submitted
Horiuchi, S., Bozek, B., Abazajian, K. N., et al. 2016, MNRAS, 456, 4346
IceCube Collaboration, Aartsen, M. G., Ackermann, M., et al. 2016, arXiv:1612.05949
Luo, B., Brandt, W. N., Xue, Y. Q., et al. 2016, arXiv:1611.03501
Marchesi, S., Civano, F., Elvis, M., et al. 2016, ApJ, 817, 34
Navarro, J. F., Frenk, C. S., & White, S. D. M. 1997, ApJ, 490, 493
Neronov, A., Malyshev, D., & Eckert, D. 2016, arXiv:1607.07328
Nesti, F., & Salucci, P. 2013, J. Cosmology Astropart. Phys., 7, 016
Moretti, A., Vattakunnel, S., Tozzi, P., et al. 2012, A&A, 548, A87
Planck Collaboration, Ade, P. A. R., Aghanim, N., et al. 2015, arXiv:1506.07135
Smith, R. K., Brickhouse, N. S., Liedahl, D. A., & Raymond, J. C. 2001, ApJ, 556, L91
Smith, R. K., Foster, A. R., & Brickhouse, N. S. 2012, Astronomische Nachrichten, 333, 301
Pal, P. B., & Wolfenstein, L. 1982, Phys. Rev. D, 25, 766
Perez, K., Ng, K. C. Y., Beacom, J. F., et al. 2016, arXiv:1609.00667
Protassov, R., van Dyk, D. A., Connors, A., Kashyap, V. L., & Siemiginowska, A. 2002, ApJ, 571, 545
Ruchayskiy, O., Boyarsky, A., Iakubovskyi, D., et al. 2016, MNRAS, 460, 1390
Shah, C., Dobrodey, S., Bernitt, S., et al. 2016, arXiv:1608.04751
Treister, E., & Urry, C. M. 2005, ApJ, 630, 115
Urban, O., Werner, N., Allen, S. W., et al. 2015, MNRAS, 451, 2447
Vikhlinin, A., Burenin, R. A., Ebeling, H., et al. 2009, ApJ, 692, 1033
Wik, D. R., Hornstrup, A., Molendi, S., et al. 2014, ApJ, 792, 48
Capak, P., Aussel, H., Ajiki, M., et al. 2007, ApJS, 172, 99
Civano, F., Marchesi, S., Comastri, A., et al. 2016, ApJ, 819, 62

Elvis, M., Civano, F., Vignali, C., et al. 2009, ApJS, 184, 158
Giacconi, R., Zirm, A., Wang, J., et al. 2002, ApJS, 139, 369
Hickox, R. C., & Markevitch, M. 2006, ApJ, 645, 95
Hickox, R. C., & Markevitch, M. 2007, ApJ, 661, L117
Luo, B., Bauer, F. E., Brandt, W. N., et al. 2008, ApJS, 179, 19-36
Luo, B., in prep.
Pal, P. B., & Wolfenstein, L. 1982, Phys. Rev. D, 25, 766
Scoville, N., Aussel, H., Brusa, M., et al. 2007, ApJS, 172, 1
Xue, Y. Q., Luo, B., Brandt, W. N., et al. 2011, ApJS, 195, 10